Clinical Cancer Research

Dual *ALK* and *CDK4/6* Inhibition Demonstrates Synergy against Neuroblastoma

Andrew C. Wood[1], Kateryna Krytska[2], Hannah T. Ryles[2], Nicole R. Infarinato[2], Renata Sano[2], Theodore D. Hansel[2], Lori S. Hart[2], Frederick J. King[3], Timothy R. Smith[3], Edward Ainscow[3], Kathryn B. Grandinetti[3], Tove Tuntland[3], Sunkyu Kim[4], Giordano Caponigro[4], You Qun He[3], Shiva Krupa[4], Nanxin Li[3], Jennifer L. Harris[3], and Yaël P. Mossé[2]

Abstract

Purpose: Anaplastic lymphoma kinase (*ALK*) is the most frequently mutated oncogene in the pediatric cancer neuroblastoma. We performed an *in vitro* screen for synergistic drug combinations that target neuroblastomas with mutations in *ALK* to determine whether drug combinations could enhance antitumor efficacy.

Experimental Design: We screened combinations of eight molecularly targeted agents against 17 comprehensively characterized human neuroblastoma-derived cell lines. We investigated the combination of ceritinib and ribociclib on *in vitro* proliferation, cell cycle, viability, caspase activation, and the cyclin D/CDK4/CDK6/RB and pALK signaling networks in cell lines with representative ALK status. We performed *in vivo* trials in CB17 SCID mice bearing conventional and patient-derived xenograft models comparing ceritinib alone, ribociclib alone, and the combination, with plasma pharmacokinetics to evaluate for drug–drug interactions.

Results: The combination of ribociclib, a dual inhibitor of cyclin-dependent kinase (CDK) 4 and 6, and the ALK inhibitor ceritinib demonstrated higher cytotoxicity ($P = 0.008$) and synergy scores ($P = 0.006$) in cell lines with *ALK* mutations as compared with cell lines lacking mutations or alterations in *ALK*. Compared with either drug alone, combination therapy enhanced growth inhibition, cell-cycle arrest, and caspase-independent cell death. Combination therapy achieved complete regressions in neuroblastoma xenografts with *ALK*-F1174L and F1245C *de novo* resistance mutations and prevented the emergence of resistance. Murine ribociclib and ceritinib plasma concentrations were unaltered by combination therapy.

Conclusions: This preclinical combination drug screen with *in vivo* validation has provided the rationale for a first-in-children trial of combination ceritinib and ribociclib in a molecularly selected pediatric population. *Clin Cancer Res; 23(11); 2856–68. ©2016 AACR.*

Introduction

Neuroblastoma is a pediatric malignancy of the sympathetic nervous system. Despite recent intensification of therapy, the long-term survival for patients with high-risk disease continues to lag significantly behind that of other common childhood cancers (1). The most frequently mutated oncogene tractable for targeted therapy is anaplastic lymphoma kinase (*ALK*), occurring as germline mutations in hereditary neuroblastomas (2, 3), and as somatically acquired mutations in sporadic disease (2–5). The most common mechanism of oncogenic *ALK* activation across all cancers is chromosomal translocation of the *ALK* tyrosine kinase domain to a homodimerization partner, including *EML4-ALK* in non–small cell lung cancer (6) and *NPM-ALK* in lymphoma (7). However, in neuroblastoma, the most common *ALK* aberrations are activating point mutations in the tyrosine kinase domain of full-length *ALK* occurring in 8% of tumors across all stages of disease (8). Within the high-risk subset of patients, the overall frequency is 14% (10% mutation, 4% amplification) at diagnosis, and the presence of an activating ALK alteration is independently prognostic of inferior outcome (8). Moreover, ALK mutations are enriched at relapse, further heightening the attractiveness of *ALK* as a tractable therapeutic target (9, 10).

Small-molecule ALK inhibitors are clinically active against malignancies with ALK translocations, (11–13), and there is known dependence of *ALK* as a driver in neuroblastoma (2–5). Yet in the pediatric phase I study of crizotinib, the objective response rate was comparatively modest in patients with relapsed neuroblastoma and activating *ALK* mutations (14). Ongoing studies examining the biochemistry of *ALK* mutations in neuroblastoma have demonstrated that crizotinib and ceritinib, as well as future generation inhibitors, face significant challenges in overcoming *ALK* mutations with innate relative resistance to ATP-competitive inhibitors, most notably at the F1174 codon (8, 12, 15). Secondary mutations at codon F1174 in translocated ALK were also associated with both acquired crizotinib resistance during preclinical *in vitro* screens (16) and progression of *ALK*-rearranged inflammatory myofibroblastic tumor (17). Although

[1]Department of Molecular Medicine and Pathology, University of Auckland, Auckland, New Zealand. [2]Division of Oncology and Center for Childhood Cancer Research, The Children's Hospital of Philadelphia, Philadelphia, Pennsylvania. [3]Genomics Institute of the Novartis Research Foundation, San Diego, California. [4]Novartis Institutes of Biomedical Research, Cambridge, Massachusetts.

Note: Supplementary data for this article are available at Clinical Cancer Research Online (http://clincancerres.aacrjournals.org/).

Corresponding Author: Yaël P. Mossé, The Children's Hospital of Philadelphia, 3501 Civic Center Boulevard, CTRB 3056, Philadelphia, PA 19104. Phone: 215-590-0965; Fax: 267-426-0685; E-mail: mosse@email.chop.edu

doi: 10.1158/1078-0432.CCR-16-1114

Translational Relevance

Activating mutations in full-length anaplastic lymphoma kinase (*ALK*) provide a drug target in the pediatric cancer neuroblastoma, but in a phase I study, an ALK inhibitor did not achieve objective responses in the majority of patients. To improve antitumor activity and durability of responses, we used high-throughput screening to identify synergistic drug combinations. The combination of a CDK4/6 and ALK inhibitor showed selective synergy and efficacy against *ALK*-mutated neuroblastomas, with dual inhibition of constitutively activated ALK and the downstream cyclin D–CDK4/6 cell cycle switch. The prevalent *ALK* F1174 hotspot mutations cause preclinical and clinical resistance to ATP-competitive ALK inhibitors; however, combined therapy achieved complete sustained regressions against F1174L xenografts. This work provides the preclinical rationale for a first-in-human trial of combination ALK and CDK4/6 inhibition in *ALK*-mutated neuroblastomas.

there is considerable enthusiasm about the preclinical data observed with lorlatinib (18), this drug has not yet been tested in children, and the toxicity profile has not been defined; in addition, single-agent kinase inhibition has often proven to be of only transient benefit.

Cancer drug development is increasingly focused on combinatorial therapies (19, 20) in recognition that single-agent tyrosine kinase inhibition frequently leads to the development of resistance and relapse (21–23). Inhibition of multiple signaling pathways is also in keeping with the current understanding of cancer cell signaling networks characterized by activation of multiple pathways, cross-talk, feedback, and redundancy (24). In metastatic melanoma with *BRAF* V600 mutations, combined BRAF and MEK pathway inhibition significantly improved survival compared with BRAF inhibition alone in treatment-naïve (25, 26) and BRAF monotherapy–resistant disease (26, 27). The use of tumor genomics to select patients suitable for combinatorial kinase inhibition is also consistent with preclinical models demonstrating that synergistic combinations are context specific (28). We postulate that targeting of key kinases and parallel pathways is necessary for cooperative and durable inhibition of ALK-mutant neuroblastoma. Therefore, we hypothesized that simultaneous inhibition of ALK and aberrant pathways may lead to superior antitumor activity in neuroblastomas with *ALK* mutations, while potentially minimizing the emergence of resistance and relapse. In this study, we sought to identify drug combinations with synergistic inhibition of *ALK*-mutated neuroblastoma cell lines by performing a pairwise combination screen of molecularly targeted agents. Here, we provide the rationale for a clinical trial of combination ceritinib (ALKi) and ribociclib (CKD4/6i) in *ALK*-driven neuroblastomas.

Materials and Methods

Cell lines and reagents

Cell lines were obtained from the Children's Hospital of Philadelphia (Philadelphia, PA) cell line bank or ATCC (Manassas, VA) and were maintained according to recommendations. Cell identity was authenticated using AmpFLSTR Identifiler (Applied Biosystems). Cells were grown to 70% to 80% confluency before experiments and plated at their predetermined cell density. Ceritinib and ribociclib were provided by Novartis, dissolved in DMSO at 10 mmol/L stock concentrations for *in vitro* experiments, and further diluted in culture medium before use.

Synergy screen

To measure the effects of chemical combinations on cell viability, cells were seeded into 1,536-well assay plates at a density of 300 cells in a 7 μL per well final volume and incubated at 37°C for approximately 18 hours before compound addition. Test compounds were prepared in a 384-well acoustic transfer compatible source plate (Labcyte) with a top concentration of 5 mmol/L, followed by an additional five 3-fold serial dilutions. Compound combinations were generated by transferring 7.5 nL of each compound/dilution from the prediluted source plates into the appropriate assay plate well using an acoustic dispenser (Labcyte ECHO555). Two replicate compound treatments were prepared for each cell line. Single-agent dose–response curves were prepared using 7.5 nL of test compound combined with 7.5 nL of DMSO to keep a consistent 0.2% DMSO concentration for all wells. Following compound addition, plates were returned to the incubator for 120 hours. Next, cellular viability was assessed by the measurement of cellular ATP levels with the addition of 3 μL per well Cell Titer-Glo (Promega), and the luminescent signal was quantitated using a ViewLux (PerkinElmer). The raw data were normalized using the signal obtained from the DMSO-treated cell control wells within each plate. Synergy score and excess synergy score calculations were performed using the Loewe additivity model based on the methods of Lehar and colleagues (28). Efficacy was calculated using the lowest normalized Cell Titer-Glo signal (maximum cytotoxicity) for a given test compound cross, regardless of compound concentration. Combination pairs that had (i) a Loewe synergy score greater than 1.75; (ii) an average Loewe excess greater than 0 across all doses tested; and (iii) a maximal cytotoxicity greater that 80% (defined as the cellular viability compared with vehicle-treated controls) were scored as being positive (Fig. 1A).

Combination index analysis assay

In vitro proliferation was measured using Real-Time Cell Sensing Impedance xCELLigence system (RT-CES, ACEA) using fixed dose molar ratios based on the D_m (absolute IC_{50}). The RT-CES is a microelectronic cell sensor system. The core of the system uses microelectronic cell sensor arrays that are integrated into the bottom of the microtiter plates. For cell-based assays, cells are grown in the individual, sensor-containing wells of the microtiter plates. The electronic sensors provide continuous, quantitative information concerning the biological status of the cells present in the well. Changes to the biological status of the cells are measured automatically and in real time by the system. Cell index values, derived from the measured impedances, are continuously displayed and plotted by the RT-CES software. Results were analyzed at 72 hours posttreatment with CalcuSyn software (Biosoft) using the combination index (CI) method developed by Chou and Talalay (29): CI <1 = synergism, 1 = additivity, and >1 = antagonism. Fraction affected is the fraction of cells inhibited by combination therapy at a given dose compared with vehicle control, where higher values indicate greater effectiveness.

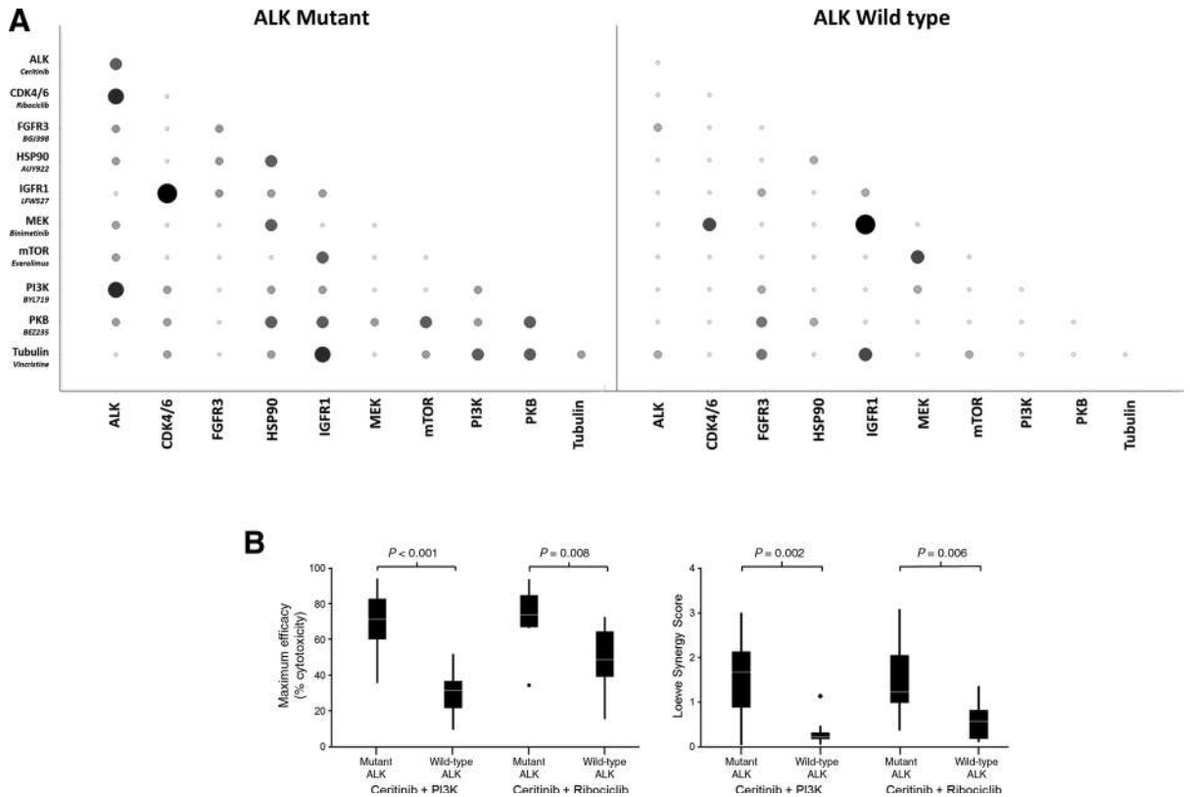

Figure 1.

ALK and CDK4/6 are synergistic drug targets in neuroblastoma. **A,** Graphical representation of the proportion of *ALK*-mutant and *ALK* wild-type cell lines screened that gave a Loewe synergy score >1.75, average Loewe excess >0, and efficacy score >0.8 with the tested compounds as single agents and in pairwise combinations. Symbol size, proportion of positive cell lines; shading, number of cell lines classified positive (white = 0, black = 3). **B,** Two combinations showed significantly increased efficacy and synergy scores in *ALK*-mutated cell lines compared with *ALK* wild-type cell lines (*P* values calculated from one-tailed *t* test).

RNAi-mediated knockdown of ALK and CDK4

NB-1691 cells were transfected with siRNA targeting ALK and CDK4 (Origene) alone or in combination, with scrambled siRNA used as a scramble. All samples were cotransfected with two siRNAs (e.g., siRNA CDK4 and siRNA CTRL, siRNA ALK and siRNA control) to ensure equal toxicity independent of their function in regulation of gene expression. Forty-eight hours after transfection, NB-1691 cells were harvested and counted using the Trypan blue exclusion method. The number of total and dead cells was calculated and results represented as fold change of dead cells normalized to the total number of cells. Subsequently, cells were evaluated for expression of phosphorylated Rb (pRB; S780) and ALK using immunoblotting analysis. β-Actin was used as loading control.

Antibodies and Western blot analysis

Cells were treated 24 hours after plating, incubated with drug for 24 hours, versenized, centrifuged, washed once with cold PBS, and stored in −80°C. Each treatment experiment was repeated 3 times. Cells were lysed on ice with hypotonic lysis buffer with protease/phosphatase inhibitor cocktail (Cell Signaling Technology) for 15 minutes and then centrifuged for 10 minutes at 4°C. The amount of protein sample was calculated using the Bradford method, and 30 to 50 μg of proteins was separated on 4%–12% Bis-Tris gradient gels, transferred to PVDF membranes (Millipore) overnight at 4°C, blocked in 5% BSA (for phosphoproteins) or 5% milk, and immunoblotted against $pALK^{Y1604}$ (Cell Signaling Technology, catalog numbers 3341S), $pALK^{Y1278}$ (6941S), total ALK (3333S), pRb^{S795} (9301S), pRb^{S780} (9307S), total Rb (9309S), cyclin D1 (2922S), cleaved caspase-3 (9664L), cleaved PARP (9541S), GAPDH (2118S), and β-actin (4967S) overnight at 4°C. All primary antibodies were diluted 1:1,000, except GAPDH and β-actin, which were diluted 1:5,000. Secondary antibodies (Santa Cruz Biotechnology) were diluted 1:10,000 and incubated, shaking, at room temperature for 1 hour. Enhanced chemiluminescence substrates were used for detection (Thermo Fisher Scientific).

Cell death, viability assays, and caspase inhibition

Cells were treated with 100 or 500 nmol/L of Actinomycin-D, or 0.5 or 1× of the D_m values of ceritinib, ribociclib, or ceritinib + ribociclib for 24 hours, plus or minus a 1-hour pretreatment with Q-VD-OPh, a caspase-3, -7, and -9 inhibitor (Sigma-Aldrich). Following 24 hours of drug incubation, cell viability was assayed with CellTiter-Glo (Promega), and paired caspase-3/7 activation was assessed using Caspase-Glo 3/7 Assay (Promega). Luminescence and fluorescence were measured on the GloMax-Multi Microplate Multimode Reader (Promega). Time course effects of caspase inhibition were determined following incubation with

vehicle, ceritinib, ribociclib, ceritinib + ribociclib, or ceritinib + ribociclib for 24, 48, or 72 hours plus or minus a 1-hour pretreatment with Q-VD-OPh (Sigma-Aldrich). Cells were stained with Trypan blue and counted using an automatic cell counter that gave the proportion of viable cells.

Cell-cycle analysis

Cell lines in 12-well plates were treated with DMSO control, equipotent serial dilutions of ceritinib or ribociclib, or equipotent combination of both drugs for 72 hours. Floating and adherent cells were collected, washed with PBS, and fixed with Fix and Perm Cell Permeabilization Kit Fixing Medium A (Life Technologies). Cell-cycle analysis was performed with FxCycle Violet Stain Kit (Life Technologies). The fixed cells were washed, and the sample concentration was adjusted to 1×10^6 cells/mL. Flow cytometry samples were prepared by adding 1 mL cell suspension and 1 μs of FxCycle Violet stain to each sample, incubated for 30 minutes, and analyzed without washing on Attune Acoustic Focusing Cytometer using 405 nm excitation and emission collected in a 450/50 bandpass or equivalent. Analysis was carried out using VenturiOne software (Applied Cytometry).

In vivo efficacy and dose reduction studies

In vivo studies were conducted on female 6- to 8-week-old CB17 SCID mice (Taconic) in adherence with the NIH Guide for the Care and Use of Laboratory Animals. The antitumor efficacy studies were conducted on mice bearing human neuroblastoma SH-SY5Y and NB-1691 xenografts, and Felix patient-derived venograft (PDX). Tumors were subcutaneously implanted into the flank of the mice for three independently performed experiments. Mice with tumors that reached 200 to 300 mm^3 were randomized into treatment arms, with 10 mice per arm. Tumors were measured using a digital caliper (Cole-Parmer) at the initiation, and one to two times per week. The absolute tumor volume (mm^3) for each group was the median of values calculated from two-dimensional tumor measurements by a spheroid formula: $(p/6) \times d3$, where d represents mean diameter. All treatments were administered orally daily 7 days per week. The SH-SY5Y and NB-1691 studies consisted of the following groups: (i) control (treated with solvent vehicle −0.5% methylcellulose, 0.5% Tween 80 in purified water); (ii) ceritinib only at 50 mg/kg dose; (iii) ribociclib only at 187.5 mg/kg (NB-1691) or 250 mg/kg in SH-SY5Y, which was reduced to 187.5 mg/kg starting on day 5 due to toxicity; and (iv) ceritinib at 50 mg/kg and ribociclib 187.5 to 250 mg/kg. Treatments were administered for 49 days. Mice were euthanized when the tumor volume reached four times its initial volume. The Felix-PDX study consisted of the following groups for 3 weeks: (i) vehicle; (ii) ceritinib at 50 mg/kg; (iii) ribociclib at 75 mg/kg; (iv) ribociclib at 125 mg/kg; (v) combination ceritinib 50 mg/kg and ribociclib 75 mg/kg; and (vi) combination ceritinib 50 mg/kg and ribociclib 125 mg/kg. Mice were euthanized when the tumor volume reached 3 cm^3. For the dose reduction study, mice bearing SH-SY5Y xenografts were treated for 3 weeks: (i) vehicle; (ii) ceritinib 50 mg/kg and ribociclib 50 mg/kg; (iii) ceritinib 50 mg/kg and ribociclib 75 mg/kg; (iv) ceritinib 50 mg/kg and ribociclib 100 mg/kg; and (v) ceritinib 50 mg/kg and ribociclib 125 mg/kg. All animal studies were approved by The Children's Hospital of Philadelphia Institutional Animal Care and Use Committee (IACUC protocol ID: IAC 15-000643).

In vivo pharmacokinetic studies

CB17 SCID female mice bearing NB-EBc1 xenografts were treated daily by oral gavage for 10 consecutive days with 50 mg/kg ceritinib, 150 mg/kg ribociclib, or both agents in combination by administering the compounds in 100 μL/10 g bodyweight. Terminal plasma samples were collected by retro-orbital bleeding from 3 mice per each time point after the final dose at 0, 4, 8, and 24 hours. Plasma concentrations of ribociclib and ceritinib were quantified using an LC/MS-MS assay.

The HPLC system, consisting of Agilent 1200 series LC binary pump (Agilent Technologies Inc.), Agilent 1200 series LC vacuum degasser (Agilent Technologies Inc.), CTCPAL_HTS autosampler (Leap Technologies), and VICI two position rotary valve (Valco Int.) was interfaced to a AB SCIEX API-4000 triple quadruple mass spectrometer (AB SCIEX). Mass spectral analyses were carried out using atmospheric pressure chemical ionization in the positive ion mode. Ribociclib (435.24 > 322.20) and ceritinib (558.30 > 433.07) were monitored using multiple reaction monitoring. Data collection and peak integration were performed using Analyst 1.4 software (SCIEX). Standard curves were generated in the concentration range of 1 ng/mL to 5,000 ng/mL. The lower limit quantitation in plasma was 1 ng/mL. The area under the plasma concentration–time curve (AUC_{0-96h}) was calculated by noncompartmental regression analysis using WinNonlin 4.0 software (Certara Inc.).

Statistical analysis for *in vivo* studies

A linear mixed-effects model was used to test the difference in the rate of tumor volume change over time between different groups. The model included group, day, and group-by-day interaction as fixed effects and included a random intercept and a random slope for each mouse. A significant group-by-day interaction would suggest that the tumor volume changes at different rates for the comparison groups. The model used vehicle group as the reference group and created separate group indicators and interaction terms for other groups. If a mouse was sacrificed or removed for biologic or biochemical analysis, the tumor volume was considered missing on the days afterward. Event-free survival (EFS) curves were estimated using Kaplan–Meier method and were compared using log-rank test. Event includes death and tumor size exceeding 3 cm^3 (mouse sacrificed). Mice that were removed for use of biology studies were considered censored at the time of removal.

Results

High-throughput screen identifies synergistic drug combinations in neuroblastoma

We evaluated 10 molecularly targeted small-molecule therapeutics, in pairwise combinations against a panel of 17 well-characterized human neuroblastoma–derived cell lines, 9 of which harbored either an activating *ALK* mutation or amplification (Table 1). Because of the large number of drug combinations and cell lines screened, we required stringent criteria to identify synergy hits and diminish experimental noise. Synergy score determination, using an algorithm based upon the Loewe additivity model (30), identified combinations of compounds that gave greater efficacy than predicted from the single-agent efficacy at the same concentrations, indicating that the compounds were interacting in a synergistic manner. A synergy score threshold of 1.75 was set to differentiate between experimentally defined additivity, that is, the activity observed when

Table 1. Drug combination screen identifies synergistic drug targets in human neuroblastoma–derived cell lines

Cell line	*ALK*[a]	*CDK4 CDK6*[a]	*MYCN* amplified[b]	*TP53*[a]	Synergy score	Maximum efficacy
LAN5[c]	R1275Q	WT	Yes	WT	3.09	0.87
NB-1643[c]	R1275Q	WT	Yes	WT	2.58	0.83
NB-SD	F1174L	WT	Yes	Mutated	2.06	0.7
COG-N-415[c]	F1174L	WT	Yes	Unknown	1.9	0.85
NB-1691	WT	*CDK4* amplified	Yes	WT *MDM2* amplified	1.36	0.73
SH-SY5Y	F1174L	WT	No	WT	1.22	0.67
KELLY	F1174L	WT	Yes	Mutated	1.19	0.74
SK-N-BE(2)	WT	WT	Yes	Mutated	1.18	0.63
NB1	Amplified and exon 2 and 3 deletion	WT	Yes	WT	0.98	0.94
LAN1	F1174L	WT	Yes	Mutated	0.96	0.66
IMR5	WT	WT	Yes	WT	0.71	0.68
SK-N-FI	WT	WT	No	Mutated	0.66	0.46
SK-N-AS	WT	WT	No	Mutated	0.48	0.52
Felix	F1245C	WT	No	WT	0.36	0.35
NLF	WT	WT	Yes	Mutated	0.2	0.43
NGP	WT	CDK4 amplified	Yes	Mutated, *MDM2* amplified	0.11	0.16
CHP134	WT	WT	Yes	WT	0.1	0.27

NOTE: Cell lines used in this study with their ALK, CDK4/6, MYCN, and p53 status. Synergy and efficacy scores obtained with ceritinib and ribociclib are noted.
[a]Defined by FoundationOne next-generation sequencing solid tumor panel.
[b]Defined by FISH.
[c]Synergy screen hit as defined by synergy score over 1.75 and maximum efficacy over 0.80.

each drug was combined with itself. A second criterion that defined screening hits was that the maximal cytotoxicity exceeded 80% cell death compared with DMSO control treatment (represented on a scale of 0–1.0). The complete dataset is presented in Supplementary Table S4.

The most active combination in both the ALK-mutant and wild-type cell lines included the IGFR1 inhibitor, LFW527, when partnered with ribociclib (CDK4/6) and binimetinib (MEK1), respectively (Fig. 1A and B; Supplementary Fig. S4). In independent studies, the combination of LFW527 and binimetinib also demonstrated robust activity in other tumor model systems (31). However, when evaluated *in vivo*, this combination demonstrated profound cytotoxicity, and no antitumor activity was observed, suggesting that LFW527 was yielding false-positive *in vitro* screening results. Therefore, we deprioritized further studies with LFW527.

Given the objectives of targeting activated *ALK* in neuroblastoma (2–5) and leveraging *ALK* mutation status as a predictive biomarker, we focused on combinations that demonstrated increased synergistic cytotoxicity when assayed on *ALK*-mutant versus *ALK* wild-type cell lines. Two combinations that did not involve LFW527 showed strong synergistic cytotoxicity in 3 or more *ALK*-mutated cell lines, while not displaying significant synergy in any of the 8 *ALK* wild-type lines: ceritinib (ALKi) and ribociclib (CDK4/6i); and ceritinib (ALKi) in combination with alpelisib (alpha isoform–specific PI3Ki; Fig. 1A). Comparison of the efficacy scores across *ALK* wild type versus mutated lines for these combinations revealed a significant bias toward greater efficacy in *ALK*-mutated lines for ceritinib in combination with alpelisib ($P < 0.001$), and ceritinib in combination with ribociclib ($P = 0.008$). In addition, both combinations showed significantly stronger synergy scores in *ALK*-mutated lines compared with *ALK* wild-type lines (ceritinib + PI3Ki, $P = 0.002$; ceritinib + ribociclib, $P = 0.006$; Fig. 1B) consistent with ceritinib driving specificity of synergy and efficacy. There did not appear to be a strong correlation between cell lines that were sensitive to the ceritinib + ribociclib and LFW527 + ribociclib combinations, suggesting that ceritinib's weak activity against IGFR1 could not account fully for its activity observed across the screening panel (Supplementary Table S4; ref. 32).

Although our initial screening criteria identified the highest-ranking responder cell lines with the strongest effects in both synergy and efficacy, the combination of ceritinib and ribociclib showed synergistic or additive cytotoxicity (i.e., greater cytotoxicity than what was observed with ceritinib and ribociclib screened as single agents) against all 9 cell lines with mutated *ALK* (Supplementary Table S1). The cell line panel contained *ALK* mutations at the three major hotspots, suggesting potential for combination activity against the majority of neuroblastomas with *ALK* aberrations. Ribociclib is an orally available, highly selective inhibitor of CDK4 and CDK6 in clinical development in numerous malignancies, including a now completed phase I clinical trial in advanced pediatric malignancies (NCT01747876) (33). On the basis of neuroblastoma tumor expression of CDK4/6 and Rb required for ribociclib activity, single-agent ribociclib activity against neuroblastoma cell lines (34), dependence of *ALK* as a driver in neuroblastoma (2–5), enrichment of synergy and efficacy in cell lines with *ALK* mutations, and the ability to use tumor *ALK* mutation status to allocate therapy, the combination of ceritinib and ribociclib was selected for further evaluation in this study.

Validation of the synergistic interaction between ALK and CDK4/6 inhibitors

To validate and extend the results of the synergy screen, we performed independent experiments in an orthogonal fashion using real-time cell impedance and calculated synergy using the Chou–Talalay method (Supplementary Table S1; ref. 29). We confirmed synergy in the three cell lines with a greater effect observed in NB-1643 with an *ALK* R1275Q mutation compared with SH-SY5Y with the comparatively ceritinib-resistant *ALK* F1174L mutation (8, 12, 15, 16). NB-1691 with *CDK4* amplification and wild-type ALK showed synergy on repeated independent experiments, but pALK was expectedly undetectable by

immunoblot, and the mechanism of interaction is unknown. To determine the direct effect of targeting ALK and CDK4, we employed siRNA to knockdown expression of ALK and CDK4 in these cells (Supplementary Fig. S3A). The knockdown of ALK increased the number of dead cells (Supplementary Fig. S3B); in contrast and as expected, the knockdown of CDK4 did not disturb cell viability (Supplementary Fig. S3B) but reduced the total number of cells as a consequence of cell-cycle arrest (Supplementary Fig. S3C). We also examined the effects of dual knockdown of ALK and CDK4 in these cells and observed a decrease in both cell viability (Supplementary Fig. S3B) and cell number (Supplementary Fig. S3C).

We then included two additional cell lines in the discovery screen that were not part of the original synergy screen (Supplementary Table S1). NB-EBc1, an *ALK* wild-type neuroblastoma cell line with robust pALK expression and *ALK* addiction (2, 15), showed synergy and efficacy at low doses. The SKNBE2C cell line with wild-type ALK, CDK4, CDK6, and intact Rb did not demonstrate synergy. Taken together, synergy was achieved in cell lines with pathogenic activation of the drug targets, consistent with an on-target mechanism.

Dual ALK/CDK4/6 inhibition enhances pALK and pRb depletion

To investigate the *in vitro* effects of combination therapy on proximal drug targets, we compared phosphoprotein signaling with single-agent and combination therapy (Fig. 2). Single-agent ALK inhibition with ceritinib caused robust dose-dependent abrogation of pALK against the most prevalent mutation, *ALK* R1275Q, in NB-1643 (Fig. 2A). Comparable pALK abrogation required higher doses in SH-SY5Y (Fig. 2B) with the *de novo* resistant ALK F1174L mutation, as reported previously (2, 8). NB-EBc1 (*ALK* WT, pALK positive) showed modest pALK abrogation with single-agent ceritinib (Fig. 2C), and NB-1691 (ALK WT, no pALK) had no detectable basal pALK expression (Fig. 2D; ref. 2). Single-agent ribociclib did not modulate pALK, even at doses over 3 μmol/L. In NB-1643, the combination of ceritinib and ribociclib enhanced abrogation of pALK compared with single-agent ceritinib, and a similar but less potent effect was evident in SH-SY5Y and NB-EBc1 (Fig. 2).

Active cyclin D–CDK4/6 complexes phosphorylate and inactivate retinoblastoma protein (Rb), causing pRb to release bound E2F transcription factors that promote expression of genes that drive progression into late G_1 and S phases. Conversely, inhibition of CDK4/6 maintains Rb in an active hypophosphorylated state so E2Fs remain bound, leading to cell-cycle arrest (33, 34). Therefore Rb hypophosphorylation is a surrogate but proximal marker of on-target CDK4/6 inhibition, although the therapeutic significance of disparate pRb status at S780 and S795 is unclear. Single-agent ribociclib caused dose-dependent abrogation of pRb in all cell lines and was most pronounced in NB-1691 with CDK4 amplification (Fig. 2A–D). In NB-1691, single-agent ALK inhibition with ceritinib had no effect on Rb phosphorylation (Fig. 2D), demonstrating that ceritinib had no off-target activity against CDK4/6 even at high doses. In contrast, in NB-1643, single-agent ALK inhibition with ceritinib decreased total Rb and abrogated pRb (Fig. 2A), consistent with pathogenic ALK signaling driving activation of the cyclin–CDK–retinoblastoma pathway. Abrogation of pRb occurred at lower doses when ribociclib was administered with ceritinib, with a less pronounced effect in other cell lines. These data suggest that ceritinib inhibited activated *ALK* and pathogenic signal transduction to CDK4/6, an effect that was augmented by ribociclib's well-characterized direct CDK4/6 inhibition.

Synergy with dual ALK–CDK4/6 inhibition is caspase and p53 independent

We next sought to determine whether the efficacy of combination therapy was dependent on intact caspase and p53 pathways, as neuroblastoma at the time of relapse is associated with disruption of caspase and TP53 programmed cell death and cytotoxic chemotherapy resistance (1, 35, 36). Cleavage of caspase-3 and PARP was detected by immunoblotting after treatment with single-agent ceritinib at pharmacologically relevant doses in all three cell lines with activated ALK: NB-1643, SH-SY5Y, and NB-EBc1 (Fig. 2A–C). Ribociclib alone did not result in detectable caspase or PARP cleavage by immunoblot, consistent with previous reports (34). Combination therapy enhanced caspase-3 and PARP cleavage at 24 hours in NB-1643 (*ALK* R1275Q), but not in other cell lines (Fig. 2A–D). To further determine mechanisms of synergy in SH-SY5Y (*ALK* F1174L), we assessed earlier time points but saw no evidence that combination treatment increased caspase cleavage (Supplementary Fig. S1A; ref. 34).

We next tested the effects of Q-VD-OPh, a potent inhibitor of caspase-3, -7, and -9 on combination therapy with ceritinib and ribociclib to further determine whether synergy was caspase dependent. Incubation of NB-1643 and SH-SY5Y with the chemotherapeutic agent Actinomycin-D for 24 hours caused potent caspase-3/7 activation and cytotoxicity. The addition of Q-VD-OPh to Actinomycin-D completely suppressed caspase activation and maintained cell viability comparable with untreated controls consistent with caspase-dependent cytotoxicity (Fig. 3A and B). Ceritinib and ribociclib monotherapy and combination therapy activated caspase-3/7 proteolysis as determined by the Caspase-Glo assay, and caspase activation was completely inhibited by the caspase inhibitor Q-VD-OPh. However, Q-VD-OPh did not protect against *in vitro* cytotoxicity caused by ceritinib alone, or combination ceritinib and ribociclib after 24 hours (Fig. 3A and B) or 72 hours (Fig. 3C and D), consistent with a caspase-independent mechanism.

TP53 activation may contribute to synergy when ALK inhibitors are combined with cytotoxic chemotherapy (37), and TP53 inactivation has been associated with neuroblastoma relapse and multidrug resistance (36). Therefore, we sought to determine whether combination ceritinib and ribociclib acted in a p53-independent manner. The combination did not result in p53 stabilization or phosphorylation, nor did it activate the downstream signaling molecule p21 compared with monotherapy or Actinomycin-D–positive controls (Supplementary Fig. S1B and S1C), excluding p53-mediated apoptosis as a mechanism of synergy. These data suggest combination ribociclib and ceritinib synergy is independent of the caspase and p53 pathways.

Dual ALK–CDK4/6 inhibition promotes cell-cycle arrest

Single-agent ribociclib performed as a cytostatic agent against human neuroblastoma–derived cell lines, leading to accumulation in the G_1 phase (34). Therefore, in cell lines where combination therapy was synergistic, we measured the proportion of cells in each phase of the cell cycle following simultaneous treatment with ribociclib and ceritinib (Supplementary Fig. S2A–S2C). Ceritinib monotherapy caused modest G_1 arrest in NB-1643 (*ALK* R1275Q) and SH-SY5Y (*ALK* F1174L) consistent

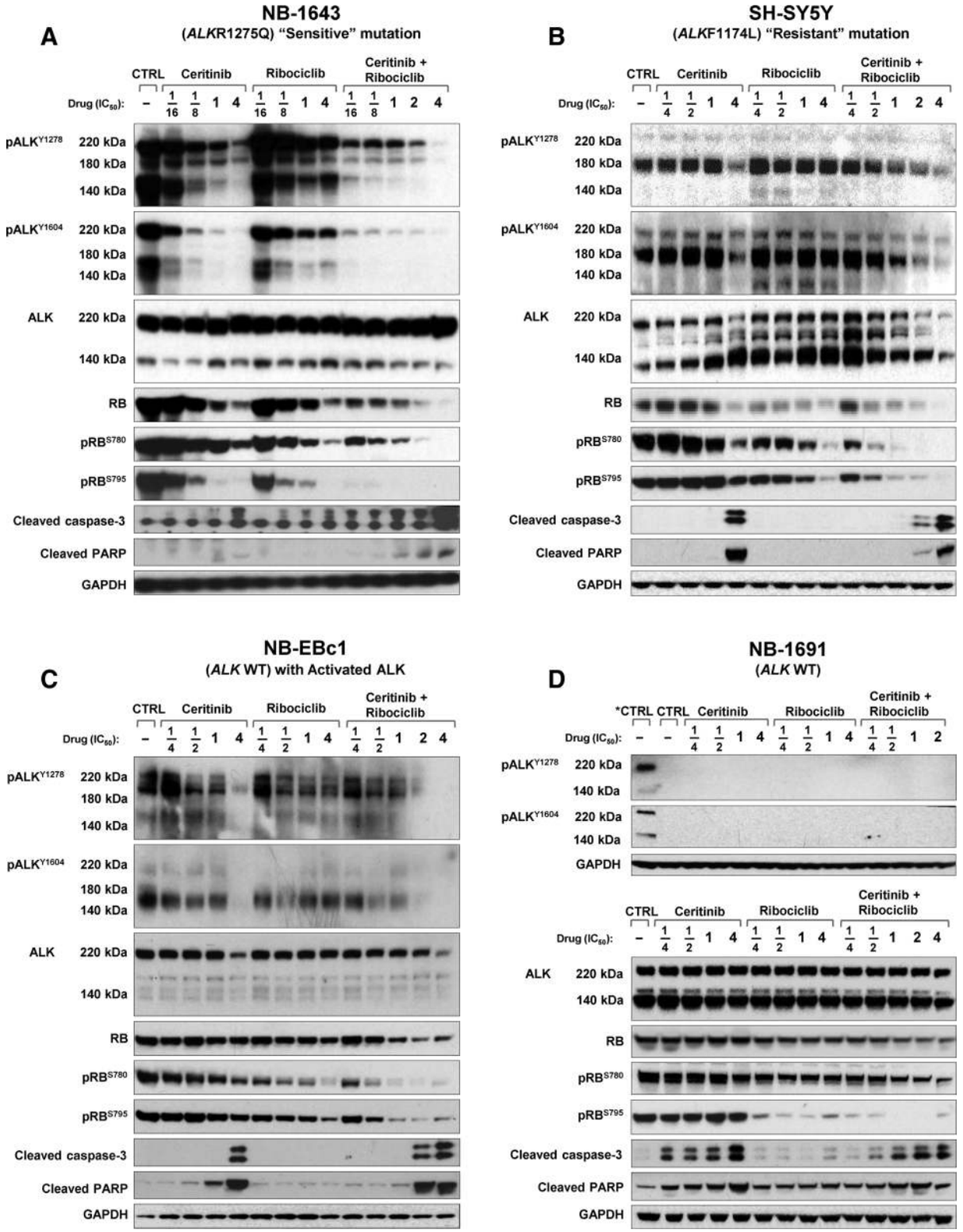

Figure 2.

Combination ALK and CDK4/6 inhibition enhances pALK and pRb depletion. Western blots of NB-1643 (**A**), SH-SY5Y (**B**), NB-EBc1 (**C**), and NB-1691 (**D**) cells treated with vehicle, ceritinib, ribociclib, or ceritinib + ribociclib at fractions of the cell lines' predetermined D_m values for each inhibitor. CTRL, control. Cells were collected for immunoblotting at 24 hours posttreatment and probed with the indicated antibodies. Untreated NB-1643 was used as a positive control for the two phospho-ALK sites on the top of **D** as NB-1691 expresses no phosphorylated ALK.

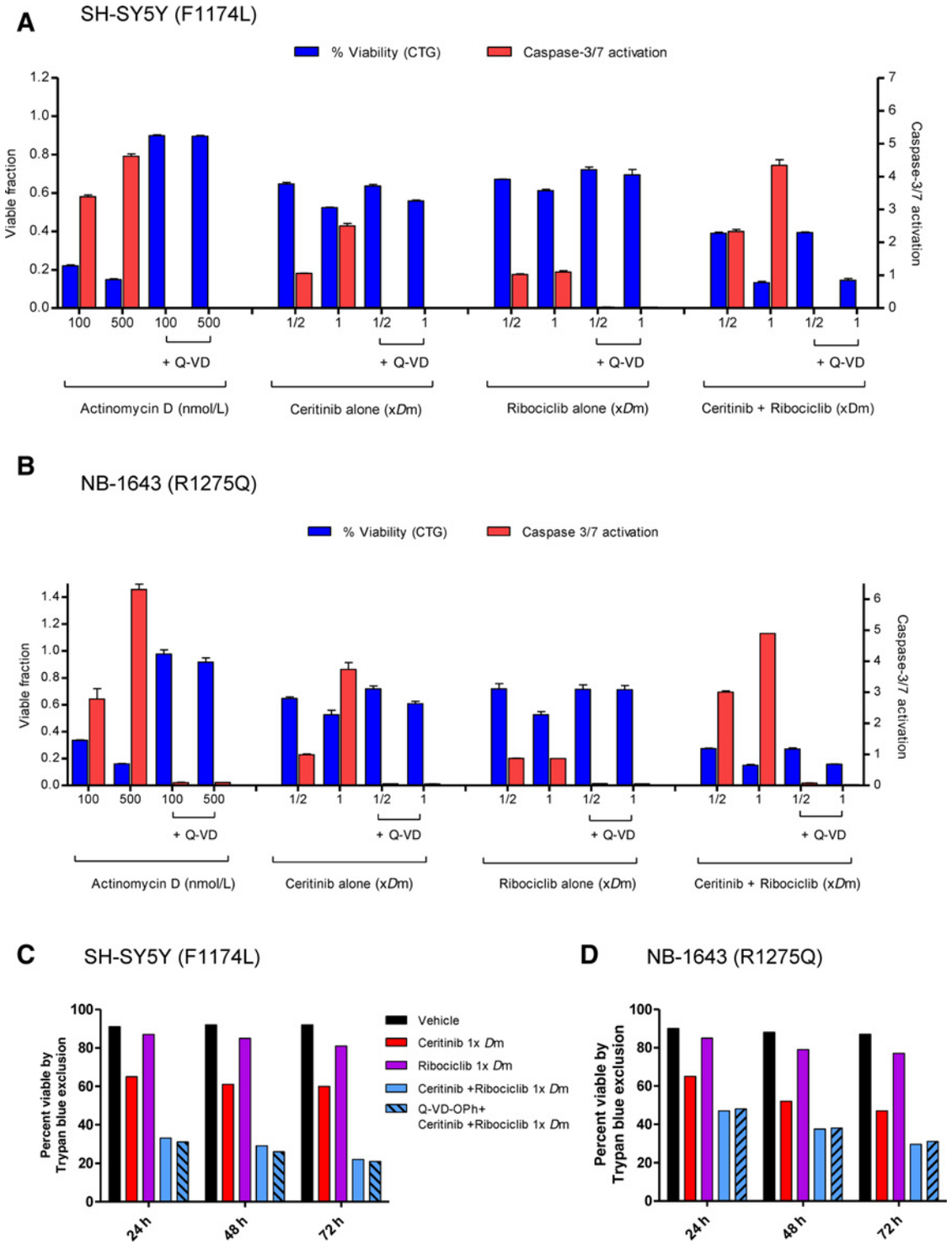

Figure 3.

Synergy between ceritinib and ribociclib in neuroblastoma cell lines does not rely on a caspase-dependent mechanism. Caspase inhibition does not restore cell viability in SH-SY5Y or NB-1643 cells *in vitro*. **A** and **B,** SH-SY5Y (**A**) and NB-1643 (**B**) cells were treated with 100 or 500 nmol/L Actinomycin-D (as a positive control), ceritinib alone, ribociclib alone, or ceritinib + ribociclib combination at 0.5 or 1× the cell's D_m value of each inhibitor. Cells were also pretreated for 1 hour with the pan-caspase inhibitor [Q-VD-OPh (Q-VD)] in the same treatment conditions. Cell viability was measured using Cell Titer-Glo (CTG), and caspase-3/7 activation was measured using Caspase-Glo 3/7 Assay Kit (Promega) at 24 hours posttreatment. **C** and **D,** SH-SY5Y (**C**) and NB-1643 (**D**) cells were treated with vehicle, ceritinib, ribociclib, or the combination at 1× the cell's D_m value of each inhibitor, with Q-VD-OPh pretreatment in a replicate of the combination treatment. Cells were collected at 24, 48, and 72 hours posttreatment to assay percentage of viable cells, measured by Trypan blue exclusion.

with CDK4 and CDK6 being downstream of activated ALK. Single-agent ribociclib caused more pronounced dose-dependent G_1 cell-cycle arrest with corresponding decreases in the fraction of cells in S and G_2–M phase. Combination therapy caused a greater accumulation in G_1 phase compared with either drug alone in all cell lines, indicating that cytostasis may have contributed to *in vitro* efficacy and synergy.

Combined ALK–CDK4/6 inhibition is effective for treatment of ALK-driven neuroblastoma xenografts

The *ALK* R1275Q mutation has lower ATP affinity compared with mutations at F1245 and F1174 codons, and R1275Q mutations were more susceptible to single-agent ATP-competitive ALK inhibitors in biochemical, preclinical, and clinical settings (8, 14, 15). Therefore, we focused initial *in vivo* experiments on the resistant *ALK* F1174L mutation using SH-SY5Y xenografts. The dose of ceritinib 50 mg/kg/daily was selected, as murine drug exposures were comparable with ceritinib exposures at the recommended dose in human adults (38). SH-SY5Y xenografts treated with ceritinib alone had prolonged EFS (Fig. 4A, $P < 0.0001$) compared with vehicle, but not growth delay ($P = 0.3$, Supplementary Table S2). SH-SY5Y xenografts treated with ribociclib (CDK4/6i) showed tumor growth delay ($P < 0.0001$) and prolonged median EFS ($P < 0.0001$) versus vehicle controls (Fig. 4A; Supplementary Table S2). All SH-SY5Y xenografts treated with combination ceritinib and ribociclib achieved complete and sustained regressions, and prolonged EFS versus either single agent ($P < 0.0001$; Fig. 4A). At predefined cessation of the study at 7 weeks, mice came off treatment and all eventually relapsed.

In NB-1691 (*ALK* WT, *CDK4* amplification), there was no benefit with single-agent ceritinib over vehicle (Fig. 4B), but single-agent ribociclib delayed tumor growth ($P < 0.0001$, statistics in Supplementary Table S2) and prolonged survival ($P < 0.0001$) compared with vehicle controls (Fig. 4B). Combination therapy significantly prolonged median survival over ribociclib monotherapy (Fig. 4B; Supplementary Table S3, $P < 0.0001$). The tumor growth linear mixed-effect analysis did not result in a statistically significant *P* value at 10 weeks of treatment, but the effectiveness of combination therapy at earlier time (1–6 weeks on treatment) shows a trend toward greater biological efficacy of combination therapy over ribociclib alone. Although NB-1691 xenografts treated with combination therapy showed complete responses, all xenografts recurred on-therapy prior to study cessation at 7 weeks (Fig. 4B).

When ribociclib human phase I pharmacokinetic data became available, the murine ribociclib doses were reduced to achieve murine plasma exposures that were pharmacologically relevant to adult human exposures. To determine whether combination therapy with reduced ribociclib doses achieved complete regressions against *ALK* F1174L xenografts, we performed a dose-finding combination study with a fixed dose of ceritinib at 50 mg/kg/daily and four different doses of ribociclib (CDK4/6i) at 50, 75, 100, and 125 mg/kg/daily for 21 days in SH-SY5Y xenografts (Fig. 4C). Ribociclib 50 mg/kg/daily in combination with ceritinib resulted in stable disease with significant tumor growth delay ($P < 0.0001$; Fig. 4C, statistics in Supplementary Table S3) and prolonged EFS (Supplementary Table S3) compared with vehicle. Combination therapy with ribociclib doses of 75, 100, and 125 mg/kg/daily resulted in complete regressions that were sustained at the *a priori* study endpoint of 3 weeks (Fig. 4C).

In our synergy screen, the cell line harboring *ALK* F1245C mutation ranked 14th of 17 cell lines with regard to synergy scores, and combination efficacy grouped with *ALK* wild-type cell lines (Table 1). Therefore, we used Felix PDXs harboring an *ALK* F1245C mutation, directly xenotransplanted from human tumor to mice without an *in vitro* intermediary step, to test the *in vivo* efficacy of combination therapy with ceritinib and ribociclib (Fig. 4D). Compared with vehicle, monotherapy with ribociclib for 3 weeks showed marginal but statistically significant tumor growth delay at both the 75 mg/kg/daily ($P = 0.01$, statistics in Supplementary Table S3) and 125 mg/kg/daily ($P = 0.001$), and superior EFS (Supplementary Table S4). Ceritinib monotherapy significantly delayed tumor progression compared with vehicle ($P < 0.0001$). The combination of ceritinib with ribociclib at either 75 mg/kg/daily or 125 mg/kg/daily doses significantly delayed tumor growth compared with ceritinib alone ($P = 0.04$) or ribociclib alone ($P < 0.0001$), and in contrast to ceritinib alone, combination therapy led to complete and sustained regressions of PDX harboring *ALK* F1245C mutations (Fig. 4D). To explore whether F1245C xenograft responses were durable, daily treatment was continued past the 3-week *a priori* endpoint until week 8. The majority of xenografts treated with ceritinib alone progressed, indicating the emergence of resistance, whereas xenografts treated with combination therapy using the ribociclib 125 mg/kg/daily dose showed sustained complete regressions.

Combination therapy did not cause drug accumulation in plasma

To evaluate whether *in vivo* efficacy was driven by plasma drug accumulation due to a drug–drug interaction, we treated CB17 SCID mice with NB-EBc1 tumor-bearing xenografts for 10 days with ceritinib 50 mg/kg/daily and ribociclib 150 mg/kg/daily either as single agents or in combination. Terminal plasma samples were obtained with 3 mice per time point after the final dose on day 10 at 0, 4, 8, and 24 hours. The steady-state plasma concentrations of ribociclib varied between 15 and 8 μmol/L, whereas those of ceritinib fluctuated between 3 and 1.9 μmol/L in the 24-hour dosing interval (Fig. 5A). There was no significant difference in plasma levels between single-agent and combination therapy with regard to maximum concentration or AUC (Fig. 5B).

Discussion

Therapy for patients with high-risk neuroblastoma continues to be optimized (39), but even in the immunotherapy era, substantial improvement is required to increase efficacy and decrease toxicity (40, 41). The discovery of activating mutations in the *ALK* oncogene in a subset of patients with high-risk neuroblastoma (8) has provided an unprecedented opportunity to impact outcome through the development of *ALK* inhibition strategies. More precise studies of clonal evolution in sequential samples from patients with neuroblastoma have revealed an emergence of *ALK* mutations at the time of relapse, a finding of utmost clinical importance given the development of *ALK* inhibition approaches (9, 10). Crizotinib inhibits *ALK* by competing with ATP for binding to its kinase active site, and we have showed that the reduced susceptibility of F1174L-mutated *ALK* to crizotinib inhibition results from its increased ATP-binding affinity (15). Our preclinical work and phase I

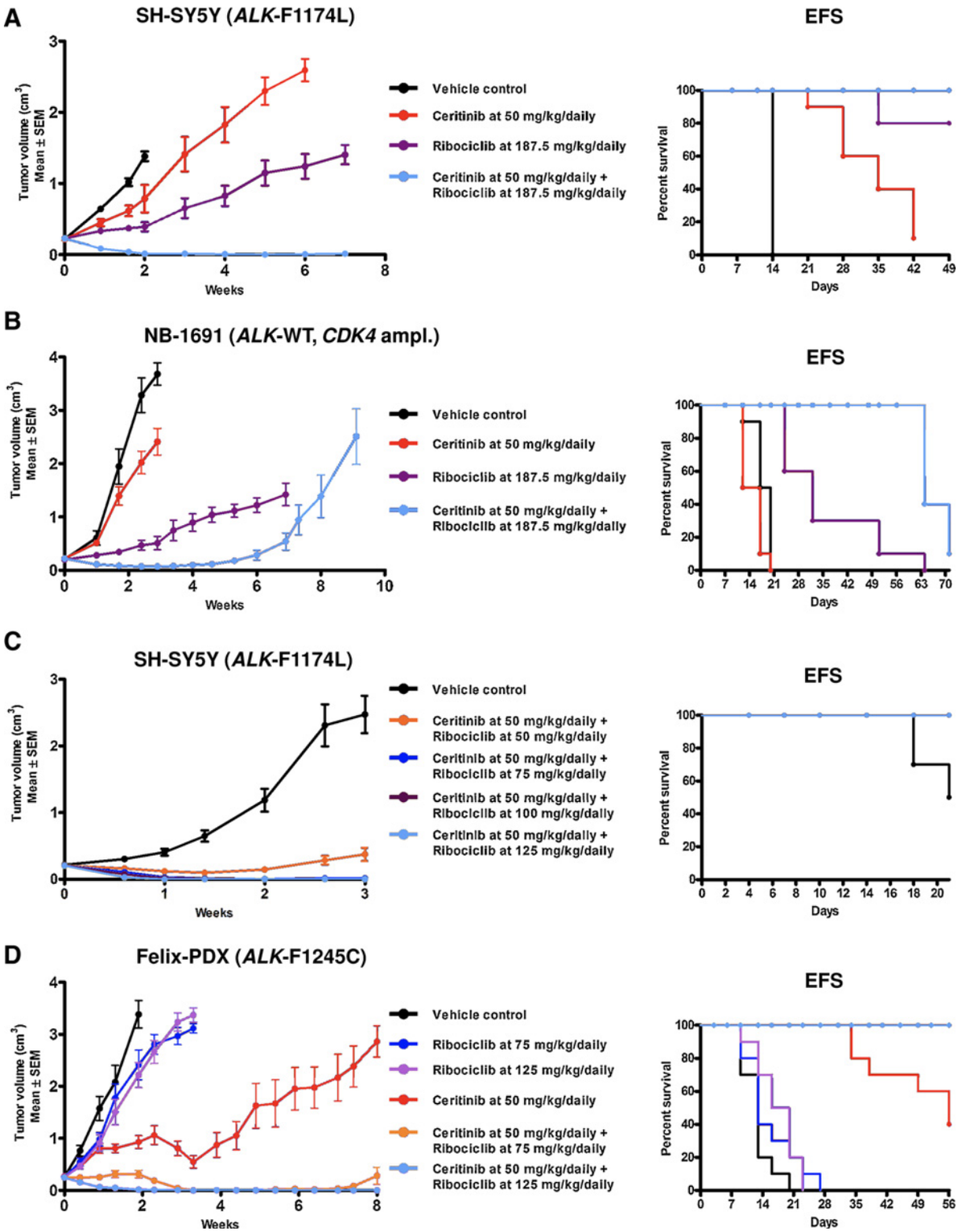

Figure 4.

Dual ALK and CDK4/6 inhibition displays marked antitumor activity in several *in vivo* models of neuroblastoma. **A–C,** Mice harboring SH-SY5Y (**A**), NB-1691 (**B**), and SH-SY5Y xenografts (**C**) were treated with vehicle or ceritinib (50 mg/kg) + four different doses of ribociclib (50, 75, 100, or 125 mg/kg) for 3 weeks. **D,** Felix-PDX tumors were treated daily orally with vehicle, ceritinib (50 mg/kg), ribociclib (75–187.5 mg/kg), or ceritinib + ribociclib for 8 weeks.

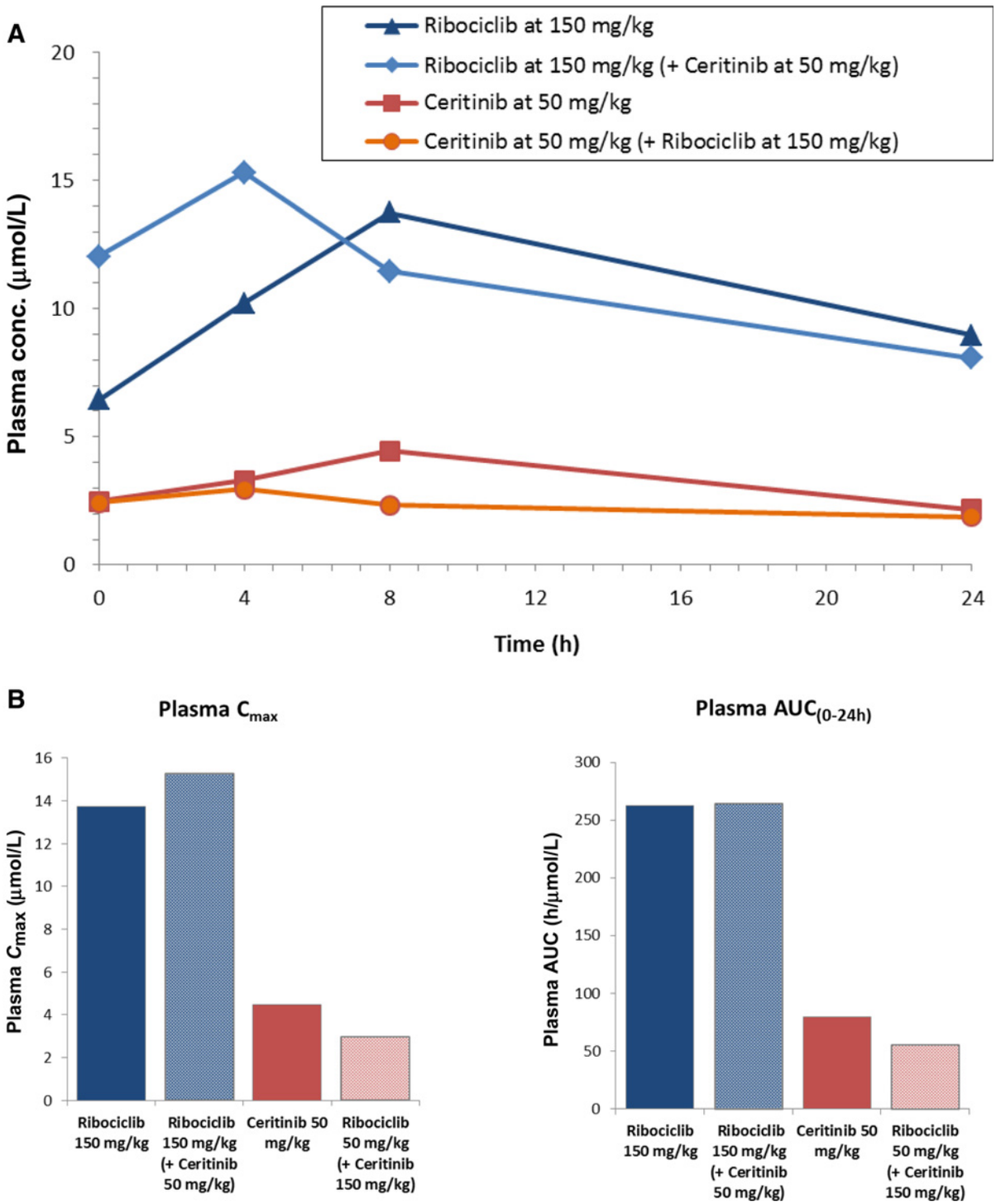

Figure 5.

Plasma was collected from CB17 SCID mice bearing NB-EBc1 xenografts and treated for 10 consecutive days to test plasma drug concentrations of monotherapy versus combination therapy. **A,** Time course of mean plasma concentrations (µmol/L) of ribociclib (LEE011) and ceritinib (LDK378) in mice ($n = 3$) on day 10 of dosing. **B,** Mean maximum plasma concentrations (C_{max}) and area under the plasma concentration time (AUC_{0-24h}) of ribociclib (LEE011) and ceritinib (LDK378) in mice ($n = 3$) on day 10 of dosing.

clinical trial of crizotinib argue that not all clinically observed *ALK* mutations are functionally relevant as *ALK* activators, and further that some ALK-activating mutations also cause primary resistance to direct *ALK* kinase inhibition with crizotinib (8, 15). Consistent with this, while marked antitumor activity was observed in patients with diseases harboring ALK translocations, far fewer objective responses were seen in patients with ALK-mutant neuroblastoma in the Children's Oncology Group phase I trial of crizotinib (14). We have therefore sought alternative ALK inhibitors, such as lorlatinib, that overcome this intrinsic resistance by simply binding more tightly to ALK (18) or by utilizing a different binding mode that is also enhanced by the mutation, or by novel–novel combination strategies.

The complexities of signaling networks that modify therapeutic vulnerability in cancer cells mandate the study of drug combinations to prevent or reverse tumor drug resistance. In melanoma, dual BRAF and MEK inhibition was superior to single-agent inhibition, with clear biological and clinical rationale to combine these agents (42, 43). These observations motivated us to identify therapeutic combinations to optimize ALK inhibition strategies in neuroblastoma. Here, we performed a cell line–based screen and focused on combinations showing selective efficacy and synergy in ALK-activated cell lines to improve the therapeutic index and durability of response. Our finding of synergy when ceritinib was combined with a PI3K inhibitor was consistent with previous reports of synergy when an ALK inhibitor was combined with a dual PI3K and mTOR inhibitor (44). We identified a novel synergistic interaction between *ALK* inhibitor ceritinib, and CDK 4/6 inhibitor ribociclib. In both active combinations identified by our synergy screen, the cell lines specifically harboring *ALK* R1275Q mutations, notably the most frequently mutated ALK residue in neuroblastoma, were highly significant, suggesting that the sensitivity of this mutation to ceritinib alone may drive combination efficacy. Although the weak activity that ceritinib has against IGF1R may contribute to the activity observed in these studies, we saw no evidence of IGF1R activation in these models. Mechanistically, we observed that the synergy from dual ALK and CDK4/6 inhibition was independent of caspase and p53 activation, and inhibition of these mechanisms has been associated with resistance to cytotoxic chemotherapeutics. We demonstrate that simultaneous ALK and CDK4/6 inhibition leads to enhanced target modulation and cell-cycle inhibition; notably, ALK inhibition only diminished phospho-Rb levels in cell lines harboring ALK activation. This is consistent with constitutive ALK signaling driving activation of CDK4 and CDK6 and suggests that ceritinib in combination with ribociclib provides upstream and downstream inhibition of the receptor tyrosine kinase and cell-cycle oncogenic network. Although it is intriguing that NB-1691, with amplification of the ribociclib target CDK4, had the highest synergy screen score of *ALK* wild-type lines, consistent with ribociclib driving the efficacy of the combination, the mechanism driving the transient antitumor activity in this model remains undefined, and our comprehensive screen data show that this particular model is broadly sensitive to RTK inhibition. Genetic knockdown of ALK and CDK4 in this cell line recapitulates the activity seen with pharmacologic inhibition and, interestingly, suggests a partial dependency on ALK that is mutation independent. Although there is currently no suitable biomarker to identify patients with wild-type ALK who may benefit from combinatorial ALK inhibition strategies, the potential oncogenic activity of wild-type ALK receptor is under further investigation. Likewise, the synergy observed in cell line EBC1 with evidence for ALK activation in the absence of a mutation or copy number alteration suggests that there may be ligand-dependent activation, a hypothesis that is being addressed.

The actionable synergistic interactions were validated using PDX models harboring *ALK* F1174L and *ALK* F1245C mutations with *de novo* crizotinib resistance and demonstrated complete and sustained tumor regressions. Murine plasma exposures associated with these responses, as best can be extrapolated to available human pharmacokinetics data, appear to be comparable with single-agent therapy in human adults. This preclinical screen in a molecularly defined subset of cell lines provided a responder hypothesis that was mechanistically validated *in vitro* and *in vivo* PDX models at pharmacologically relevant doses. These data provide the preclinical rationale for a first-in-children biomarker-driven trial of dual ALK and CDK4/6 inhibition in a pediatric population with shared molecular etiology driven by the presence of an underlying activating ALK lesion.

Disclosure of Potential Conflicts of Interest

No potential conflicts of interest were disclosed.

Authors' Contributions

Conception and design: A.C. Wood, K. Krytska, L.S. Hart, T.R. Smith, S. Kim, G. Caponigro, N. Li, J.L. Harris, Y.P. Mossé

Development of methodology: A.C. Wood, K. Krytska, T.R. Smith, J.L. Harris, Y.P. Mossé

Acquisition of data (provided animals, acquired and managed patients, provided facilities, etc.): A.C. Wood, K. Krytska, H.T. Ryles, N.R. Infarinato, T.D. Hansel, F.J. King, T.R. Smith, K.B. Grandinetti, J.L. Harris, Y.P. Mossé

Analysis and interpretation of data (e.g., statistical analysis, biostatistics, computational analysis): A.C. Wood, K. Krytska, H.T. Ryles, N.R. Infarinato, F.J. King, T.R. Smith, E. Ainscow, T. Tuntland, S. Kim, G. Caponigro, Y.Q. He, N. Li, J.L. Harris, Y.P. Mossé

Writing, review, and/or revision of the manuscript: A.C. Wood, K. Krytska, H.T. Ryles, R. Sano, F.J. King, T.R. Smith, E. Ainscow, T. Tuntland, G. Caponigro, N. Li, J.L. Harris, Y.P. Mossé

Administrative, technical, or material support (i.e., reporting or organizing data, constructing databases): K. Krytska, F.J. King, T.R. Smith, E. Ainscow, J.L. Harris, Y.P. Mossé

Study supervision: T.R. Smith, G. Caponigro, J.L. Harris, Y.P. Mossé

Other (project and alliance management): S. Krupa

Acknowledgments

We thank members of the Mossé laboratory and Novartis/GNF colleagues for valuable discussions.

Grant Support

This work was supported in part by the NIH (grant R01-CA140198; to Y.P. Mossé), the Alex's Lemonade Stand Foundation REACH award (to Y.P. Mossé), the St Baldrick's Foundation Fellow award (to A.C. Wood), and the George L. Ohrstrom Jr. Foundation (to A.C. Wood).

The costs of publication of this article were defrayed in part by the payment of page charges. This article must therefore be hereby marked *advertisement* in accordance with 18 U.S.C. Section 1734 solely to indicate this fact.

Received May 1, 2016; revised November 29, 2016; accepted December 1, 2016; published OnlineFirst December 16, 2016.

References

1. Maris JM. Recent advances in neuroblastoma. N Engl J Med 2010;362: 2202–11.
2. Mosse YP, Laudenslager M, Longo L, Cole KA, Wood A, Attiyeh EF, et al. Identification of ALK as a major familial neuroblastoma predisposition gene. Nature 2008;455:930–5.
3. Janoueix-Lerosey I, Lequin D, Brugieres L, Ribeiro A, de Pontual L, Combaret V, et al. Somatic and germline activating mutations of the ALK kinase receptor in neuroblastoma. Nature 2008;455:967–70.
4. Chen Y, Takita J, Choi YL, Kato M, Ohira M, Sanada M, et al. Oncogenic mutations of ALK kinase in neuroblastoma. Nature 2008;455:971–4.
5. George RE, Sanda T, Hanna M, Frohling S, Luther WII, Zhang J, et al. Activating mutations in ALK provide a therapeutic target in neuroblastoma. Nature 2008;455:975–8.
6. Soda M, Choi YL, Enomoto M, Takada S, Yamashita Y, Ishikawa S, et al. Identification of the transforming EML4-ALK fusion gene in non-small-cell lung cancer. Nature 2007;448:561–6.
7. Morris SW, Kirstein MN, Valentine MB, Dittmer KG, Shapiro DN, Saltman DL, et al. Fusion of a kinase gene, ALK, to a nucleolar protein gene, NPM, in non-Hodgkin's lymphoma. Science 1994;263:1281–4.
8. Bresler SC, Weiser DA, Huwe PJ, Park JH, Krytska K, Ryles H, et al. ALK mutations confer differential oncogenic activation and sensitivity to ALK inhibition therapy in neuroblastoma. Cancer Cell 2014;26: 682–94.
9. Eleveld TF, Oldridge DA, Bernard V, Koster J, Daage LC, Diskin SJ, et al. Relapsed neuroblastomas show frequent RAS-MAPK pathway mutations. Nat Genet 2015;47:864–71.
10. Schleiermacher G, Javanmardi N, Bernard V, Leroy Q, Cappo J, Rio Frio T, et al. Emergence of new ALK mutations at relapse of neuroblastoma. J Clin Oncol 2014;32:2727–34.
11. Tartari CJ, Scapozza L, Gambacorti-Passerini C. The ALK gene, an attractive target for inhibitor development. Curr Top Med Chem 2011;11:1406–19.
12. Friboulet L, Li N, Katayama R, Lee CC, Gainor JF, Crystal AS, et al. The ALK inhibitor ceritinib overcomes crizotinib resistance in non-small cell lung cancer. Cancer Discov 2014;4:662–73.
13. Shaw AT, Engelman JA. ALK in lung cancer: past, present, and future. J Clin Oncol 2013;31:1105–11.
14. Mosse YP, Lim MS, Voss SD, Wilner K, Ruffner K, Laliberte J, et al. Safety and activity of crizotinib for paediatric patients with refractory solid tumours or anaplastic large-cell lymphoma: a Children's Oncology Group phase 1 consortium study. Lancet Oncol 2013;14:472–80.
15. Bresler SC, Wood AC, Haglund EA, Courtright J, Belcastro LT, Plegaria JS, et al. Differential inhibitor sensitivity of anaplastic lymphoma kinase variants found in neuroblastoma. Sci Transl Med 2011;3:108ra14.
16. Zhang S, Wang F, Keats J, Zhu X, Ning Y, Wardwell SD, et al. Crizotinib-resistant mutants of EML4-ALK identified through an accelerated mutagenesis screen. Chem Biol Drug Des 2011;78:999–1005.
17. Sasaki T, Okuda K, Zheng W, Butrynski J, Capelletti M, Wang L, et al. The neuroblastoma-associated F1174L ALK mutation causes resistance to an ALK kinase inhibitor in ALK-translocated cancers. Cancer Res 2010;70: 10038–43.
18. Infarinato NR, Park JH, Krytska K, Ryles HT, Sano R, Szigety KM, et al. The ALK/ROS1 inhibitor PF-06463922 overcomes primary resistance to crizotinib in ALK-driven neuroblastoma. Cancer Discov 2016;6:96–107.
19. Bozic I, Reiter JG, Allen B, Antal T, Chatterjee K, Shah P, et al. Evolutionary dynamics of cancer in response to targeted combination therapy. Elife 2013;2:e00747.
20. Woodcock J, Griffin JP, Behrman RE. Development of novel combination therapies. N Engl J Med 2011;364:985–7.
21. Nguyen KS, Kobayashi S, Costa DB. Acquired resistance to epidermal growth factor receptor tyrosine kinase inhibitors in non-small-cell lung cancers dependent on the epidermal growth factor receptor pathway. Clin Lung Cancer 2009;10:281–9.
22. Kobayashi S, Ji H, Yuza Y, Meyerson M, Wong KK, Tenen DG, et al. An alternative inhibitor overcomes resistance caused by a mutation of the epidermal growth factor receptor. Cancer Res 2005;65:7096–101.
23. Shi H, Hong A, Kong X, Koya RC, Song C, Moriceau G, et al. A novel AKT1 mutant amplifies an adaptive melanoma response to BRAF inhibition. Cancer Discov 2014;4:69–79.
24. Lee MJ, Ye AS, Gardino AK, Heijink AM, Sorger PK, MacBeath G, et al. Sequential application of anticancer drugs enhances cell death by rewiring apoptotic signaling networks. Cell 2012;149:780–94.
25. Robert C, Karaszewska B, Schachter J, Rutkowski P, Mackiewicz A, Stroiakovski D, et al. Improved overall survival in melanoma with combined dabrafenib and trametinib. N Engl J Med 2015;372:30–9.
26. Long GV, Stroyakovskiy D, Gogas H, Levchenko E, de Braud F, Larkin J, et al. Combined BRAF and MEK inhibition versus BRAF inhibition alone in melanoma. N Engl J Med 2014;371:1877–88.
27. Johnson DB, Flaherty KT, Weber JS, Infante JR, Kim KB, Kefford RF, et al. Combined BRAF (dabrafenib) and MEK inhibition (trametinib) in patients with BRAFV600-mutant melanoma experiencing progression with single-agent BRAF inhibitor. J Clin Oncol 2014;32:3697–704.
28. Lehar J, Krueger AS, Avery W, Heilbut AM, Johansen LM, Price ER, et al. Synergistic drug combinations tend to improve therapeutically relevant selectivity. Nat Biotechnol 2009;27:659–66.
29. Chou TC. Drug combination studies and their synergy quantification using the Chou-Talalay method. Cancer Res 2010;70:440–6.
30. Boik JC, Newman RA, Boik RJ. Quantifying synergism/antagonism using nonlinear mixed-effects modeling: a simulation study. Stat Med 2008; 27:1040–61.
31. Gao H, Korn JM, Ferretti S, Monahan JE, Wang Y, Singh M, et al. High-throughput screening using patient-derived tumor xenografts to predict clinical trial drug response. Nat Med 2015;21:1318–25.
32. Marsilje TH, Pei W, Chen B, Lu W, Uno T, Jin Y, et al. Synthesis, structure-activity relationships, and in vivo efficacy of the novel potent and selective anaplastic lymphoma kinase (ALK) inhibitor 5-chloro-N2-(2-isopropoxy-5-methyl-4-(piperidin-4-yl)phenyl)-N4-(2-(isopropylsulf onyl)phenyl) pyrimidine-2,4-diamine (LDK378) currently in phase 1 and phase 2 clinical trials. J Med Chem 2013;56:5675–90.
33. Sherr CJ, Beach D, Shapiro GI. Targeting CDK4 and CDK6: from discovery to therapy. Cancer Discov 2016;6:353–67.
34. Rader J, Russell MR, Hart LS, Nakazawa MS, Belcastro LT, Martinez D, et al. Dual CDK4/CDK6 inhibition induces cell-cycle arrest and senescence in neuroblastoma. Clin Cancer Res 2013;19:6173–82.
35. Goldsmith KC, Gross M, Peirce S, Luyindula D, Liu X, Vu A, et al. Mitochondrial Bcl-2 family dynamics define therapy response and resistance in neuroblastoma. Cancer Res 2012;72:2565–77.
36. Tweddle DA, Pearson AD, Haber M, Norris MD, Xue C, Flemming C, et al. The p53 pathway and its inactivation in neuroblastoma. Cancer Lett 2003;197:93–8.
37. Krytska K, Ryles HT, Sano R, Raman P, Infarinato NR, Hansel TD, et al. Crizotinib synergizes with chemotherapy in preclinical models of neuroblastoma. Clin Cancer Res 2016;22:948–60.
38. Shaw AT, Kim DW, Mehra R, Tan DS, Felip E, Chow LQ, et al. Ceritinib in ALK-rearranged non-small-cell lung cancer. N Engl J Med 2014; 370:1189–97.
39. Matthay KK, Reynolds CP, Seeger RC, Shimada H, Adkins ES, Haas-Kogan D, et al. Long-term results for children with high-risk neuroblastoma treated on a randomized trial of myeloablative therapy followed by 13-cis-retinoic acid: a children's oncology group study. J Clin Oncol 2009; 27:1007–13.
40. Hobbie WL, Moshang T, Carlson CA, Goldmuntz E, Sacks N, Goldfarb SB, et al. Late effects in survivors of tandem peripheral blood stem cell transplant for high-risk neuroblastoma. Pediatr Blood Cancer 2008; 51:679–83.
41. Oeffinger KC, Mertens AC, Sklar CA, Kawashima T, Hudson MM, Meadows AT, et al. Chronic health conditions in adult survivors of childhood cancer. N Engl J Med 2006;355:1572–82.
42. Flaherty KT, Infante JR, Daud A, Gonzalez R, Kefford RF, Sosman J, et al. Combined BRAF and MEK inhibition in melanoma with BRAF V600 mutations. N Engl J Med 2012;367:1694–703.
43. Ribas A, Gonzalez R, Pavlick A, Hamid O, Gajewski TF, Daud A, et al. Combination of vemurafenib and cobimetinib in patients with advanced BRAF(V600)-mutated melanoma: a phase 1b study. Lancet Oncol 2014;15: 954–65.
44. Moore NF, Azarova AM, Bhatnagar N, Ross KN, Drake LE, Frumm S, et al. Molecular rationale for the use of PI3K/AKT/mTOR pathway inhibitors in combination with crizotinib in ALK-mutated neuroblastoma. Oncotarget 2014;5:8737–49.